A Virtual Over-the-Air Method for 5G Massive MIMO Base Station Testing With Flexible Virtual Probes

HUAQIANG GAO[1], **WEIMIN WANG**[1], **YONGLE WU**[1], **YUANAN LIU**[1], **AND GERT FRØLUND PEDERSEN**[2]

[1]Beijing Key Laboratory of Work Safety Intelligent Monitoring, Department of Electronic Engineering, Beijing University of Posts and Telecommunications, Beijing 100876, China
[2]Department of Electronic Systems, Faculty of Engineering and Science, Antenna Propagation and Millimeter-Wave Systems Section, Aalborg University, 9220 Aalborg, Denmark

Corresponding author: Weimin Wang (wangwm@bupt.edu.cn)

ABSTRACT Massive multiple-input–multiple-output (MIMO) is known as a large-scale antenna technology and has been enabled for the fifth generation (5G) mobile communication systems. The over-the-air (OTA) testing of massive MIMO antenna system has attracted a lot of attention in terms of evaluating the radio performance of a 5G base station (BS). As a promising OTA test methodology, the sectored multi-probe anechoic chamber (MPAC) setup is employed for the performance testing of massive MIMO BS. However, the system cost and installation are still an issue to be considered in practice (e.g., the anechoic chamber and multiple probes), though it can accurately reconstruct the flexible propagation channels by channel emulation methods. This paper proposes a virtual OTA test framework for the performance testing of massive MIMO BS on the basis of MPAC setups. As an alternative, the proposed virtual OTA test system adopting the concept of virtual probes solves the inconveniences and limitations of the actual probe installation in MPAC setups. The BS array responses to the actual probes of MPAC setups are generated in a phase matrix for the virtual probes. First, in this paper, the system description of virtual OTA testing is given. Then, the emulation method of spatial clusters is presented for the virtual OTA testing. Finally, simulations are performed with good channel emulation accuracy.

INDEX TERMS Massive multiple-input multiple-output (MIMO) testing, multi-probe anechoic chamber (MPAC), channel emulation, virtual over-the-air (OTA) testing, virtual probes.

I. INTRODUCTION

The fifth generation (5G) wireless telecommunication systems are currently in standardization phase [1]–[3]. In 5G communications, massive multiple-input multiple-output (MIMO) has been utilized as an enabling technique [4]–[6]. Many antenna elements are employed at the base station (BS) side to help achieve high rate transmission to multiple simultaneous users. Performance evaluation of massive MIMO BS is an essential step in different development stages. Unlike legacy 4G MIMO with limited number of antennas [7]–[9],

performance testing of massive MIMO BS would in theory require much more probes and hardware resources.

The performance testing of massive MIMO BS with over-the-air (OTA) method has been reported in the literature [10]–[12]. As a more suitable method than other two methodologies (i.e. reverberation chamber (RC) based methods [13], [14] and radiated two-stage (RTS) methods [15]–[17]), the multi-probe anechoic chamber (MPAC) based test system is employed for the OTA testing of massive MIMO BS [18]. Further, a sectored MPAC setup is applied, where a sectored probe configuration is defined. Much work on the sectored MPAC OTA test setup has been reported in the literature [18]–[22]. The main work is briefly introduced in the following.

The associate editor coordinating the review of this manuscript and approving it for publication was Giorgio Montisci.

The applicability of three 4G OTA test methods is discussed for massive MIMO BS testing in [18]. The spatial correlation errors are assessed for various 2D channel models in 2D MPAC setups with uniform and sectored configurations. It concludes that the OTA probe number and the setup dimension can be greatly reduced in sectored configurations than uniform configurations. Reference [19] investigates physical dimensions of MPAC setups in terms of saving space cost and proposes a 3D sectored MPAC setup for massive MIMO BS performance evaluation. Simulation results are given for the impact of measurement distance on various metrics to determine the range of sectored MPAC setups. It is concluded that the measurement distance can be decreased with no need to meet conventional far field criteria. Finally, [22] elaborates on a comprehensive 3D sectored MPAC method for massive MIMO BS testing. Simulations are conducted to determine key design parameters of 3D sectored MPAC setups in terms of several new metrics. The general idea of 3D sectored MPAC OTA setups for massive MIMO BS testing is to select probe locations and determine probe weights in the context of prefaded signal synthesis (PFS) or plane wave synthesis (PWS) method. A limited number of active probe antennas are selected to radio channel emulator (CE) by switching within specific sector of space angle. The specific sector is covered by a large number of actual probe antennas (called probe wall in the following). Power weights and complex weights are determined on spatial correlation error and field synthesis error within the test area for the PFS method and the PWS method, respectively. The PWS method focuses on the synthesis of individual subpath, while the cluster composed of multiple subpaths is emulated by the PFS method.

As introduced above, the system cost of MPAC setups is a major concern in terms of chamber size and the number of OTA probes associated with CE hardware resources. Compared with the conventional MPAC setup, the proposed 3D sectored MPAC setup is more attractive for massive MIMO BS testing due to smaller chamber dimension and fewer active radio frequency (RF) chains of the CE. But still, for the 3D sectored MPAC setup, it might be cost-prohibitive and complicated in practical installations of the anechoic chamber and the probe wall and the implementation of the switching circuitry. Challenges for the existing 3D sectored MPAC setup are briefly discussed in the following.

From point of view of OTA probes, one challenge lies in the limited angular coverage of probe wall. The sectored probe wall only covers a part of the power angular spectrum (PAS) of target channel model. Even if it can cover one target PAS with concentrated distribution with respect to the center of probe wall regardless of rotating the device under test (DUT) or not, there is no guarantee that it will cover another when the channel model is updated. Further, for the target PAS distributed dispersedly (e.g. 3D clustered delay line model A in 3GPP [23]), the selection of active probes is very limited and even ineffective in terms of emulation accuracy, which would lead to large deviations in the channel emulation. Also, it is very inconvenient and almost impossible in practice to change the fixed sectored probe wall with the various channel spatial profiles. If we increase the coverage of probe wall to cover much more directions regardless of the channel spatial profiles, the difficulty of installing probe wall would be increased than the limited coverage of probe wall, though the probes are cheap. In this case, the size of switching circuitry is also increased as limited number of active probes need to be selected within the probe wall. Meanwhile, the rest of unselected probes increased needs to be inactive by load. In addition, probe angular spacing within probe wall will be small for the target clustered PAS with narrow cluster angular spreads to ensure good emulation accuracy. In this situation, antenna coupling between active OTA probes is another issue to be considered in practice. From point of view of chamber size, another challenge is the far-field requirement. The distance between OTA probes and DUT is far enough to ensure plane waves impinging on the DUT in an ideal MPAC setup. However, the chamber size is too limited to meet the requirement for the electrically large massive MIMO BS in practice.

Alternatively, on the basis of the 3D sectored MPAC setup, the probe wall, the switching circuitry, and the anechoic chamber can be substituted by a phase matrix. The function of active OTA probes to emulate spatial cluster characteristics in sectored MPAC setups is equivalent to the far-field array responses (phase rotation of signals received at DUT elements), which can be realized by a phase matrix. It seems like that the phase matrix achieves the virtual probes at the corresponding locations of actual probes. Consequently, the limitations related with OTA probes in sectored MPAC setups are non-existent for the virtual probes. Also, the limitations relative with chamber size does not exist in the virtual OTA testing because the far-field array response is simply carried out in the phase matrix.

It would be attractive to test massive MIMO BS adopting this concept of virtual probes accomplished by a phase matrix. The concept of virtual probes is adopted here to emphasize the role of the phase matrix (i.e. collocating probes fictitiously). Very limited work in the literature has addressed this aspect. A conductive massive MIMO testing is briefly described in [24] using a combination of a phase matrix and a CE, but no detailed algorithm is given. In this paper, a virtual OTA method (or called the virtual probes method) for 5G massive MIMO BS testing is proposed using the virtual probes based on an MPAC method. The virtual probes are carried out by a phase matrix. The row dimension and the column dimension of the phase matrix are the number of DUT elements and virtual probes, respectively. The proposed virtual OTA testing method overcomes the challenges mentioned above in the 3D sectored MPAC setup. The main contributions of this paper lies in following aspects:

1) Challenges for the existing 3D sectored MPAC setup is discussed for massive MIMO BS testing and a virtual OTA test framework using virtual probes is proposed based on an MPAC method.

2) The functionality of actual probes of MPAC setups is substituted by the virtual probes in a phase matrix and the possible ways of connection between phase matrix and DUT array are discussed in the virtual OTA test system.

3) The channel emulation method of spatial clusters is presented for the virtual OTA testing with good emulation accuracy in terms of the spatial correlation, the PAS estimate, and the beam probability.

The rest of the paper is organized as follows. In Section II, the proposed OTA test system is described on the basis of MPAC setups. In Section III, the emulation method of spatial clusters is presented for the virtual OTA testing and three evaluation metrics are revisited. In Section IV, simulations are given in terms of the spatial correlation, the PAS estimate, and the beam probability. Conclusion is given in Section V.

The notation used in this paper is as follows: $(\cdot)$ denotes the vector dot product or scalar multiplication operator, $\|\cdot\|_1$ the first-order norm, $\|\cdot\|_2$ the second-order norm, $E\{\cdot\}$ the expectation operator, $\{\cdot\}^*$ the complex conjugate operator. Scalars are shown in regular font, while vectors and matrices are in bold font.

II. VIRTUAL OTA TEST SYSTEM

In this section, the virtual OTA test system is proposed for 5G massive MIMO BS testing on the basis of an MPAC method. The focus is on the sub-6 GHz bands of 5G frequency allocations. The uplink transmission is selected as an example in the fading emulation to illustrate its principle. The BS in receive mode is to be tested by testing signals created by user equipment (UE) or UE emulator. Identical with the 3D sectored MPAC setup in the literature shown in Fig. 1(a), path power and delay, fading, multipath spread, and cross polarization power ratio can be emulated in the CE. However, the OTA probes emulating the spatial clusters seen by BS are replaced by the virtual probes which are achieved by a phase matrix in the proposed virtual OTA test system.

A system diagram of the proposed virtual OTA testing is presented in Fig. 1(b), where the basic idea is to accomplish the functionality of actual OTA probes of MPAC setups by a phase matrix. The actual probes in ideal MPAC setups produce the far-field phase rotation at DUT array elements. The far-field array response of M DUT elements created by K actual probes with different spatial locations are realized by phase control in the phase matrix. In other words, setting the array responses to K actual probes in the phase matrix is to collocate K virtual probes at the corresponding locations of actual probes, which is very flexible. The power of K virtual probes are provided by K CE outputs. The received signals at locations of M DUT elements are provided by M outputs of the phase matrix. For this reason, the phase matrix includes K inputs and M outputs. K inputs are for K virtual probes (i.e. K CE outputs), while M outputs are for M DUT elements. The phase control is on each input to output connection in the phase matrix. As demonstrated in Fig. 1(b),

each output m of the phase matrix to DUT element m is a combination of phase rotation from K inputs. Each input k of phase matrix from CE output k is split to M outputs of the phase matrix. Note that the phase control (phase information) on each input to output connection in the phase matrix is realized by a phase shifter. The phase shifter is for the single-frequency or narrowband signal in the phase matrix. For a broadband signal, the phase information in the phase matrix changes with frequency. In this case, multiple phase shifters are needed in the phase control on each input to output connection. Therefore, a broadband signal needs multiple phase matrix resources than a single-frequency or narrow-band signal. In this paper, one phase shifter for the phase control on each input to output connection in the phase matrix is considered for simplicity to illustrate the basic principle of the proposed virtual OTA method.

The conductive connection is simply adopted from the CE to the phase matrix, while the connection to DUT array from the phase matrix can be conducted in a conductive mode or an OTA mode. It is a straightforward way to connect them directly by conductive cables with element patterns bypassed in a conductive mode, assuming that separate RF chains are provided for DUT elements (e.g. the situation when BS array elements ports are available on sub 6 GHz bands of 5G frequency allocations). The OTA mode is to locate the DUT array in a small RF shielded enclosure, as shown in Fig. 2. OTA antennas are equipped inside the enclosure, with antenna ports outside. A calibration matrix G is introduced between the phase matrix and the enclosure. The inputs and the outputs of calibration matrix G are connected to the phase matrix outputs and the OTA antenna ports, respectively. The $M \times M$ calibration matrix G is adopted to calibrate out the $M \times M$ transfer matrix A between M OTA antennas and M DUT elements, i.e the product AG of the calibration matrix G and the transfer matrix A can be approximate to a identity matrix I. In practice, a large enough isolation level between crosstalk link and direct link is expected to ensure the test accuracy and repeatability, and to neglect the uncertainties on test accuracy caused by crosstalk. Finally the desired direct link from the phase matrix to the DUT elements are established. In this approach, it refers to the idea of wireless cable in the second stage of RTS OTA testing [15]–[17], while it essentially differs from the RTS method. The virtual OTA testing based on an MPAC method still virtually has the advantage of the MPAC method.

In addtion, there is a very ideal method in an OTA mode, i.e., each output m of the phase matrix is equipped with a directive OTA antenna m. The OTA antenna patterns are highly directive so that each DUT element m only receives signals from the corresponding antenna m, without undesired crosstalk from others, i.e. achieving desired direct link. However, such a directive antenna doesn't exist in practice because very narrow beamwidth (i.e. half power beam width, HPBW) is required to avoid undesired crosstalk. For example, DUT array element spacing is 5 cm (half wavelength at 3 GHz), the distance from DUT array to a directive antenna is 1 m.
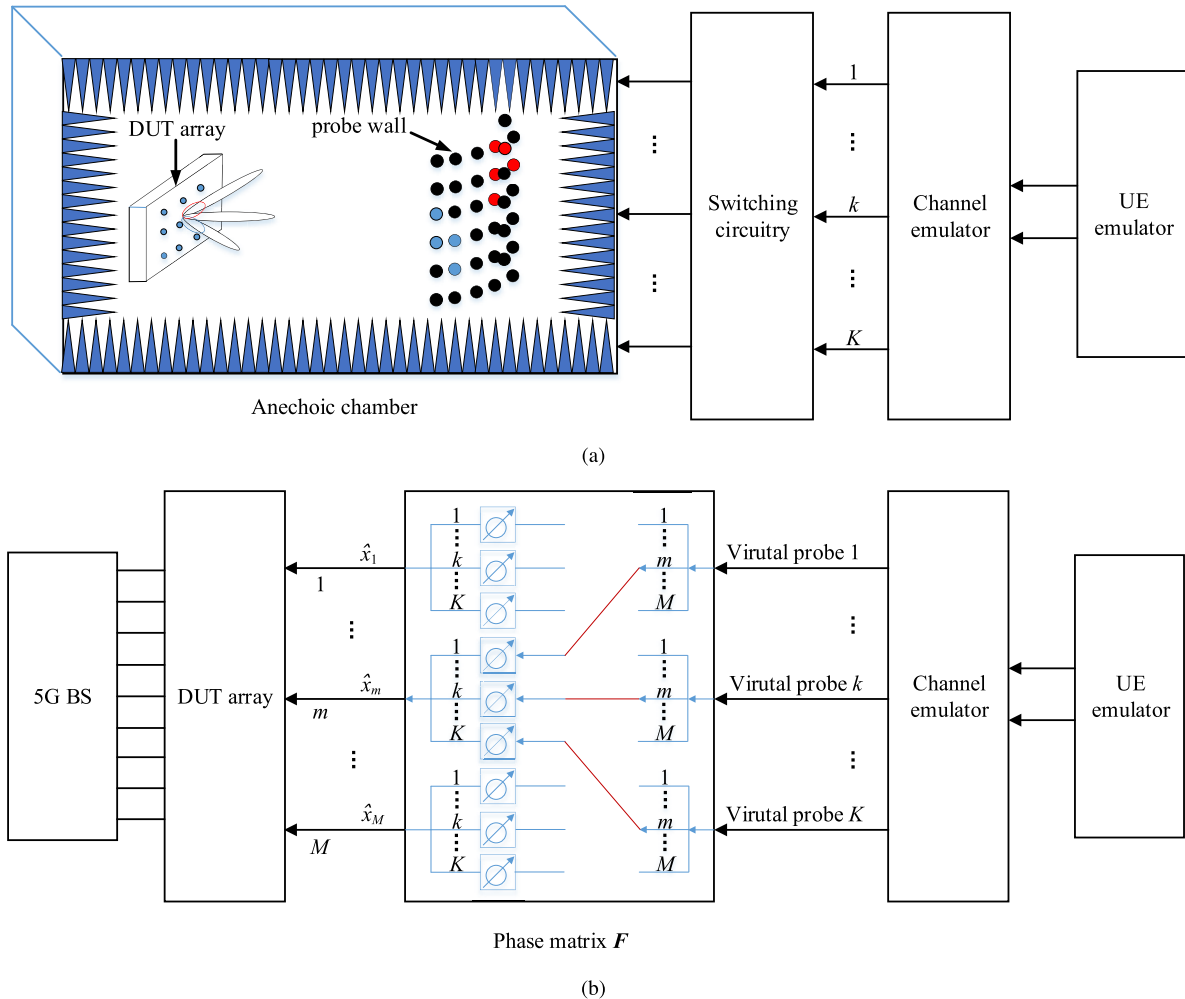
(a)

(b)

FIGURE 1. An illustration of test systems for massive MIMO BS performance evaluation. (a) A 3D sectored MPAC OTA setup [22]. (b) Proposed virtual OTA test system, where the connection from *K* inputs to the *m*th output is highlighted in a phase matrix for illustration.

In this case, the directive antenna should have a maximal HPBW of 2.8° to avoid undesired crosstalk. In practice, it is very difficult for the directive antenna that the HPBW is smaller than 10°.

It is noted that practical aspects related to the proposed test system, e.g. DUT element ports connection in conductive modes, alignment and calibration in OTA modes, implementation of the phase matrix, etc., are not discussed in the paper. The focus is on the principle illustration of the proposed virtual OTA test system based on the 3D sectored MPAC setups.

To further highlight the advantages of the proposed virtual OTA method, comparisons with the reported OTA methods are listed in Table 1.

III. CHANNEL EMULATION FOR VIRTUAL OTA TESTING

In this section, the PFS emulation technique in MPAC setups is selected as an example due to its advantage of emulating the geometry-based stochastic channel model (GSCM, cluster-based channel model). The main point is on the extension for the virtual OTA testing of massive MIMO BS. A single
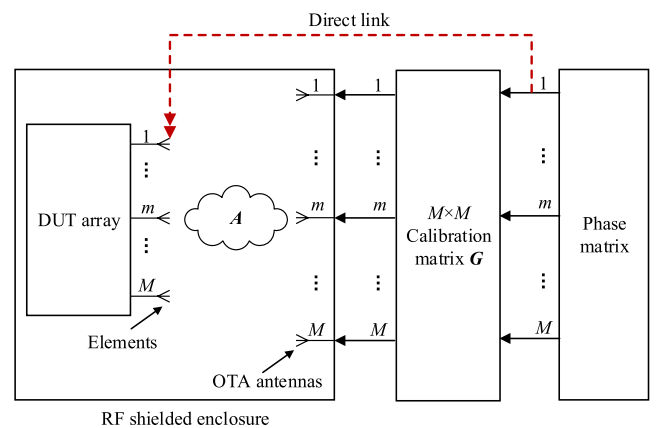

FIGURE 2. OTA connection from the phase matrix to DUT array in the proposed virtual OTA test system.

polarization is considered for simplicity in the PFS technique as the same PAS of target channel models can be reproduced for both horizontal and vertical polarizations. Further,

TABLE 1. Comparisons with the reported OTA methods.

Methods	OTA probes	Chamber	Channel model	Cost	Complexity
RC [14]	Yes	Reverberative	Isotropic	Low	Low
RTS [15]	Yes	Anechoic	Flexible	Medium	Medium
MPAC [18], [22]	Multiple	Anechoic	Arbitrary	High	High
Proposed work	No	No	Arbitrary	Medium	Medium

the focus of study is on the reconstruction of spatial angular structure of channel model at the DUT side, i.e. PAS of spatial clusters. Note that the concept of MIMO OTA testing is to first reconstruct the target wireless channel environment in a certain area, and then the entire DUT is placed within the area to be tested over the air (i.e. OTA). Generally, a key point in the MIMO OTA testing is the channel reconstruction (i.e. channel emulation). Once the channel is emulated properly, the subsequent performance testing (e.g. throughput) can be guaranteed. Therefore, the focus of this paper is on the virtual OTA test system configuration and the channel emulation, instead of the practical testing procedure.

A. PHASE MATRIX FOR VIRTUAL PROBE LOCATION

In this part, the phase matrix is constructed by determining the locations of virtual probes. A probe selection framework is reported in [25] for MPAC setups. It gives that good channel emulation accuracy can be attained by adopting limited OTA probes from all available probes. The same results are also found in [22]. Different from [25] and [22], the virtual probe locations in this paper are unstinted, so the probe selection from restricted probes set is no longer suitable for the virtual probes. On the other hand, the virtual probes can be seen as an extreme case of [25] and [22] where the available probes are infinite. So it is still not possible to use the selection algorithms here for determining the probe locations. In addition, the results in [25] verifies that the selected probes match well with the angles of arrival of spatial clusters. In [26], it is suggested that the PFS method remaps the cluster with small angular spread to its closest probes for a better emulation accuracy. Also in [22], dominant clusters are favored by probes.

Therefore, a simple and effective method of determining the virtual probe locations is presented in the following just based on the cluster power and its space angle. The target multi-cluster channel model with L clusters is considered. $\boldsymbol{P} = \{P_l\} \in \mathbb{R}^{L \times 1}$ denotes a vector of L cluster powers. $\boldsymbol{\phi} = \{\phi_l\} \in \mathbb{R}^{L \times 1}$ and $\boldsymbol{\theta} = \{\theta_l\} \in \mathbb{R}^{L \times 1}$ denote the vector of azimuth angles of departure (AoDs) and elevation angles of departure (EoDs) of L clusters, respectively. The azimuth angles and the elevation angles for K virtual probes are denoted as $\hat{\boldsymbol{\phi}} = \{\hat{\phi}_k\} \in \mathbb{R}^{K \times 1}$ and $\hat{\boldsymbol{\theta}} = \{\hat{\theta}_k\} \in \mathbb{R}^{K \times 1}$, respectively. Note that K is confined to not more than the number of clusters with different AoDs in this part for simplicity in case K is large.

First, re-sort L clusters of the target channel model in descending order of their powers $\boldsymbol{P}$. Based on the new order

of clusters, then K different AoDs and EoDs from the first cluster to the last cluster are designated as the azimuth angles $\hat{\boldsymbol{\phi}}$ and the elevation angles $\hat{\boldsymbol{\theta}}$ of K virtual probes, respectively. The detailed procedure of determining K probe locations is summarized in Algorithm 1.

Algorithm 1 Procedure of Determining the Virtual Probe Locations

---

Input: $\boldsymbol{P}$, $\boldsymbol{\phi}$, $\boldsymbol{\theta}$, and K
Output: $\hat{\boldsymbol{\phi}}$ and $\hat{\boldsymbol{\theta}}$

2   Sort the elements P_l of $\boldsymbol{P}$ in descending order;
3   Collect a index vector $\boldsymbol{c} = \{c_l\} \in \mathbb{C}^{L \times 1}$ for describing the arrangement of the elements of $\boldsymbol{P}$ into the sorted vector;
4   Initialize $\hat{\boldsymbol{\phi}} \leftarrow \boldsymbol{0}$ and $\hat{\boldsymbol{\theta}} \leftarrow \boldsymbol{0}$;
5   Set $s \leftarrow c_1$, $\hat{\phi}_1 \leftarrow \phi_s$, $\hat{\theta}_1 \leftarrow \theta_s$;
6   Set $k \leftarrow 2$ and $l \leftarrow 2$;
7   **while** $k \leq K$ **do**
8      $s \leftarrow c_l$;
9   **if** $\phi_s \in \hat{\boldsymbol{\phi}}$ **then**
10        $\hat{\phi}_k \leftarrow \phi_s$;
11        $\hat{\theta}_k \leftarrow \theta_s$;
12        $k \leftarrow k + 1$;
13   **end**
14      $l \leftarrow l + 1$;
15   **end**
16   Return $\hat{\boldsymbol{\phi}}$ and $\hat{\boldsymbol{\theta}}$

With the determined locations $\hat{\boldsymbol{\phi}}$ and $\hat{\boldsymbol{\theta}}$ of K virtual probes, the phase matrix $\boldsymbol{F}$ is constructed as

$$\boldsymbol{F} = \{f_{m,k} = e^{j\frac{2\pi}{\lambda}\vec{r_m}\cdot\vec{\hat{\Omega}}_k}\} \in \mathbb{C}^{M \times K}, \tag{1}$$

where $\vec{\hat{\Omega}}_k$ is the kth unit position vector denoting the space angle $\hat{\Omega}_k = (\hat{\phi}_k, \hat{\theta}_k)$ of the kth virtual probe. $\vec{r_m}$ is a unit position vector of the mth DUT element. M and K are the number of DUT elements and virtual probes, respectively.

Note that the phase matrix $\boldsymbol{F}$ is applied for all clusters in this study for simplicity, though it can be updated for each cluster. Also, for dynamic channel models with time-variant spatial profiles, the real-time updating of virtual probe locations can be carried out in the programmable phase matrix. Nevertheless, each cluster of wideband multi-cluster channel is still emulated individually with independent power weights optimization in the following.

B. WEIGHT OPTIMIZATION FOR VIRTUAL PROBE POWER

After the phase matrix $\boldsymbol{F}$ is determined, the next step is to decide the power weights of K virtual probes in the CE. As mentioned in the literature [22], a straightforward method of direct sampling target PAS by probe locations does not produce optimal weights because of not considering DUT aperture. In the following is adopted minimizing the spatial correlation error in terms of 3D channel spatial characteristics. Optimization algorithm is used as an example in this

study, though a computationally effective method to minimize PAS deviation for dynamic channel models is described in [27].

The target received signal $x_m(t)$ at the location of the mth DUT element is a linear summation of contributions from the continuous power distributions of target channel model. It is expressed for each cluster l (with pathloss ignored for simplicity, as it's identical for all elements in the far field), as

$$x_m^{(l)}(t) = \oint e^{j\frac{2\pi}{\lambda}\vec{r_m}\cdot\vec{\Omega}} \sqrt{P^{(l)}(\Omega)} e^{j\varphi_\Omega(t)} \, d\Omega, \quad (2)$$

where $x_m^{(l)}(t)$ is the target received signal from the lth cluster. $\vec{\Omega}$ is a unit vector denoting space angle Ω. $P^{(l)}(\Omega)$ is the PAS of the lth target cluster with power $P_l = \oint P^{(l)}(\Omega) \, d\Omega$. $e^{j\varphi_\Omega(t)}$ denotes the independent and identically distributed (i.i.d.) fading signals from the far-field of target channel.

Since the spatial correlation is defined as a statistical measure of signal similarity, the target spatial correlation at any pair $q = (u, v)$ of spatial locations $\vec{r_u}$ and $\vec{r_v}$ for DUT element u and v respectively ($u, v \in [1, M]$) is expressed for the lth cluster as

$$\rho_q^{(l)} = \frac{1}{\mu_l} E\left\{ x_u^{(l)}(t) \cdot x_v^{(l)}(t)^* \right\}$$
$$= \frac{1}{P_l} \oint e^{j\frac{2\pi}{\lambda}(\vec{r_u}-\vec{r_v})\cdot\vec{\Omega}} P^{(l)}(\Omega) \, d\Omega, \quad (3)$$

where $\mu_l = P_l$ is the scaling constant to satisfy $\rho_q^{(l)} = 1$ when $u = v$ for the lth cluster. The detailed derivation for (3) is given in Appendix A-A.

As presented in Section II, the mth output of the phase matrix is the emulated spatial signal $\hat{x}_m(t)$ at the location of DUT element m. The emulated signal $\hat{x}_m(t)$ is a linear summation of contributions from discrete K virtual probes transmitting weighted fading signals. For the lth cluster of the emulated channel, it is expressed as

$$\hat{x}_m^{(l)}(t) = \sum_{k=1}^{K} e^{j\frac{2\pi}{\lambda}\vec{r_m}\cdot\vec{\Omega}_k} \sqrt{\hat{P}_k^{(l)}} e^{j\varphi_k(t)}, \quad (4)$$

where $\hat{x}_m^{(l)}(t)$ is the spatial signal at the mth DUT element from the lth emulated cluster. $e^{j\frac{2\pi}{\lambda}\vec{r_m}\cdot\vec{\Omega}_k} = f_{m,k}$ is the response of the mth DUT element to the kth virtual probe. $\hat{P}_k^{(l)}$ is the power of the kth virtual probe for the lth emulated cluster provided by the kth CE output. The lth emulated cluster has the same power $P_l = \sum_{k=1}^{K} \hat{P}_k^{(l)}$ as the target one. $e^{j\varphi_k(t)}$ denotes the i.i.d. fading signals transmitted from the kth CE output.

The corresponding spatial correlation at locations pair q for the lth emulated cluster is written as

$$\hat{\rho}_q^{(l)} = \frac{1}{\hat{\mu}_l} E\left\{ \hat{x}_u^{(l)}(t) \cdot \hat{x}_v^{(l)}(t)^* \right\}$$
$$= \frac{1}{P_l} \sum_{k=1}^{K} \hat{P}_k^{(l)} \cdot e^{j\frac{2\pi}{\lambda}(\vec{r_u}-\vec{r_v})\cdot\vec{\Omega}_k}$$
$$= \sum_{k=1}^{K} w_k^{(l)} \cdot e^{j\frac{2\pi}{\lambda}(\vec{r_u}-\vec{r_v})\cdot\vec{\Omega}_k}, \quad (5)$$

where $\hat{\mu}_l = P_l$ is the scaling constant to satisfy $\hat{\rho}_q^{(l)} = 1$ when $u = v$ for the lth emulated cluster. Here, $w_k^{(l)} = \hat{P}_k^{(l)}/P_l$ is the power weight of the kth virtual probe for the lth emulated cluster. $\sum_{k=1}^{K} w_k^{(l)} = 1$ is satisfied. Appendix B-A gives the detailed derivation for (5).

The power weight $w_k^{(l)}$ in (5) is obtained by convex optimization [28] in the following for each cluster separately (i.e. L convex optimizations)

$$\boldsymbol{w}^{(l)} = \arg\min \left\| \boldsymbol{\rho}^{(l)} - \hat{\boldsymbol{\rho}}^{(l)} \right\|_2, \quad (6)$$

where $\boldsymbol{w}^{(l)} = \{w_k^{(l)}\} \in \mathbb{R}^{K\times 1}$ is a optimized power weighting vector normalized to sum of unity for each cluster l. $\boldsymbol{\rho}^{(l)} = \{\rho_q^{(l)}\} \in \mathbb{C}^{Q\times 1}$ and $\hat{\boldsymbol{\rho}}^{(l)} = \{\hat{\rho}_q^{(l)}\} \in \mathbb{C}^{Q\times 1}$ are the target and the emulated spatial correlation vector, respectively. Here, $q = (u, v)$ ($u \neq v$) represents a pair of any two different locations among M DUT elements. The dimension of spatial correlation vector is $Q = \binom{M}{2}$.

C. EVALUATION METRICS

Three evaluation metrics [22] of channel emulation for 5G OTA testing are revisited detailedly in this part. Specifically, the metrics are presented under the narrowband multi-cluster channel model for example (i.e. multiple clusters are combined without delay distinction), though they can also be presented for each cluster individually.

1) SPATIAL CORRELATION ERROR

This metric evaluates how well the emulated channel is reproduced in terms of the spatial correlation characteristics.

First the target spatial correlation for the narrowband multi-cluster channel model is

$$\rho_q = \frac{1}{\mu} E\left\{ x_u(t) \cdot x_v(t)^* \right\}$$
$$= \frac{1}{\mu} \sum_{l'=1}^{L} \sum_{l=1}^{L} \oint e^{j\frac{2\pi}{\lambda}(\vec{r_u}-\vec{r_v})\cdot\vec{\Omega}} \sqrt{P^{(l)}(\Omega)P^{(l')}(\Omega)} \, d\Omega, \quad (7)$$

where μ is the scaling constant to satisfy $\rho_q = 1$ when $u = v$ for the target narrowband multi-cluster channel. The detailed derivation for (7) is provided in Appendix A-B.

Similarly, the emulated spatial correlation is

$$\hat{\rho}_q = \frac{1}{\hat{\mu}} E\left\{ \hat{x}_u(t) \cdot \hat{x}_v(t)^* \right\}$$
$$= \frac{1}{\hat{\mu}} \sum_{l'=1}^{L} \sum_{l=1}^{L} \sum_{k=1}^{K} \sqrt{\hat{P}_k^{(l)}\hat{P}_k^{(l')}} \cdot e^{j\frac{2\pi}{\lambda}(\vec{r_u}-\vec{r_v})\cdot\vec{\Omega}_k}$$
$$= \frac{1}{\hat{\mu}} \sum_{l'=1}^{L} \sum_{l=1}^{L} \sum_{k=1}^{K} \sqrt{P_l P_{l'}} \sqrt{w_k^{(l)}w_k^{(l')}} \cdot e^{j\frac{2\pi}{\lambda}(\vec{r_u}-\vec{r_v})\cdot\vec{\Omega}_k}, \quad (8)$$

where $\hat{\mu}$ is the scaling constant to satisfy $\hat{\rho}_q = 1$ when $u = v$ for the emulated narrowband multi-cluster channel. Appendix B-B provides the detailed derivation for (8).

As stated in [29], the high spatial correlation has more influence on the MIMO performance than the low spatial

correlation. Then correlation error weighted by target spatial correlation is applied to emphasize the influence, i.e. weighted root mean square (rms) error e_ρ defined as

$$e_\rho = \sqrt{\frac{\sum_{q=1}^{Q} |\rho_q - \hat{\rho}_q|^2 \cdot |\rho_q|}{\sum_{q=1}^{Q} |\rho_q|}}. \qquad (9)$$

2) TOTAL VARIATION DISTANCE OF PAS
This metric evaluates how well the emulated PAS matches the target PAS, as seen by the DUT array with limited aperture. It is related to both the PAS structure and the DUT array aperture. The PAS seen by the DUT is obtained by estimation algorithms. A Bartlett beamforming algorithm is used as an example, though a multiple signal classification (MUSIC) algorithm is also described in [30]. Then the estimated PAS is given for the target and the emulated channel, respectively by

$$P_{est}(\Omega) = \boldsymbol{a}^H(\Omega)\boldsymbol{R}\boldsymbol{a}(\Omega), \qquad (10)$$

$$\hat{P}_{est}(\Omega) = \boldsymbol{a}^H(\Omega)\hat{\boldsymbol{R}}\boldsymbol{a}(\Omega), \qquad (11)$$

where $\boldsymbol{R} = \{\rho_{u,v}\} \in \mathbb{C}^{M \times M}$ and $\hat{\boldsymbol{R}} = \{\hat{\rho}_{u,v}\} \in \mathbb{C}^{M \times M}$ denote the target and the emulated spatial correlation matrix between two DUT elements u and v ($u, v \in [1, M]$), respectively. $\boldsymbol{a}(\Omega) = \{a_m(\Omega) = e^{j\frac{2\pi}{\lambda} \vec{r}_m \cdot \vec{\Omega}}\} \in \mathbb{C}^{M \times 1}$ is the array response vector of DUT steering for the estimated space angle Ω.

Next, the estimate error of normalized PAS to sum of unity (i.e. total variation distance of PAS) is calculated as

$$D_{est} = \frac{1}{2} \int \left| \frac{P_{est}(\Omega)}{\int P_{est}(\Omega') \, d\Omega'} - \frac{\hat{P}_{est}(\Omega)}{\int \hat{P}_{est}(\Omega') \, d\Omega'} \right| d\Omega. \qquad (12)$$

3) BEAM STATISTICAL DISTANCE
This metric evaluates the similarity of beam probability distributions under the target and the emulated channel model. The beam probability is recently investigated to characterize the selection performance under spatial channels for 5G antenna systems [22], [31], [32]. It demonstrates the probability distribution of the beam with the strongest power over all fading snapshot. The beam direction is selected among all predefined directions for each snapshot.

The beam probability p_b of the bth beam under the target channel model is defined as

$$p_b = \frac{n_b}{N}, \qquad (13)$$

where n_b is the time for the bth beam with the strongest power over N snapshots under the target channel model. b is the beam index.

The bth beam with the strongest power at the nth snapshot is

$$b[n] = \arg\max P_{beam}(\Omega_b)[n], \qquad (14)$$

where Ω_b denotes space angle of bth beam direction. $P_{beam}(\Omega_b)[n]$ is the power of the bth main beam pointing to the space angle Ω_b using Bartlett beamforming at the nth snapshot, expressed as

$$P_{beam}(\Omega_b)[n] = \left| \boldsymbol{a}^H(\Omega_b)\boldsymbol{x}[n] \right|^2, \qquad (15)$$

where $\boldsymbol{x}[n] = \{x_m[n]\} \in \mathbb{C}^{M \times 1}$ is a vector containing M received signals of DUT at the nth snapshot under the target channel model. $\boldsymbol{a}^H(\Omega_b) = \{e^{-j\frac{2\pi}{\lambda} \vec{r}_m \cdot \vec{\Omega}_b}\} \in \mathbb{C}^{1 \times M}$ is the weights vector of M DUT elements for Bartlett beamforming in the beam direction Ω_b.

Similar to (13)$\sim$(15), the emulated beam probability $\hat{p}_b$ of the bth beam is obtained with the received signal vector $\hat{\boldsymbol{x}}[n] = \{\hat{x}_m[n]\} \in \mathbb{C}^{M \times 1}$ of DUT under the emulated channel.

Beam statistical distance is adopted to measure the beam probability error suitably, as discussed in [32]. The beam statistical distance between the target and the emulated beam probability distributions is calculated by

$$D_{beam} = \frac{1}{2} \left\| \boldsymbol{p} - \hat{\boldsymbol{p}} \right\|_1, \qquad (16)$$

where $\boldsymbol{p} = \{p_b\} \in \mathbb{C}^{B \times 1}$ and $\hat{\boldsymbol{p}} = \{\hat{p}_b\} \in \mathbb{C}^{B \times 1}$ are the target and the emulated beam probability vector, respectively. B is the number of predefined beams.

IV. SIMULATION SETTINGS AND RESULTS
In this section, simulations are given following the principle of Section III. In simulation settings, DUT is a uniform planar array with half wavelength spacing both in horizontal and vertical direction. As indicated in Section III-A, the virtual probe locations determined in this paper are more suitable for narrower cluster of the target channel to attain better emulation accuracy. Hence, the 3D clustered delay line (CDL) C model with small cluster angular spread is referred to as the target channel, which is clear and well defined in [23].

In simulation results, the stated metrics of Section III-C is demonstrated to evaluate emulation accuracy for two DUT sizes (i.e. a 8×8 array and a 16×16 array). In addition, 16 virtual probes are selected as an example in the simulation for the limited RF ports of the CE in practice. Although multiple CEs can be combined to increase the available RF ports, it still increases the setup cost dramatically.

A. VIRTUAL PROBES AND PHASE MATRIX
Since the locations of virtual probes are determined by the PAS of the target channel, Fig. 3 shows the target PAS and the corresponding locations of virtual probes. In addition, the target PAS is mapped to $[-90°, 90°]$ in azimuth angle symmetrically as two directions symmetric with respect to the DUT array plane cannot be distinguished by the DUT. It can be seen that 16 probe locations are allocated at the center of 16 dominant clusters with different AoDs and EoDs. The DUT array has no rotation with respect to probes because propagation clusters with any direction in the target channel model can be directly emulated by the flexible virtual probes.
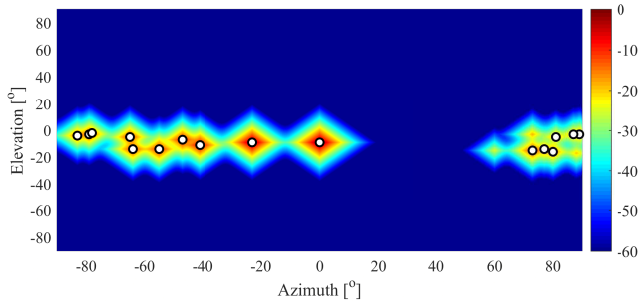
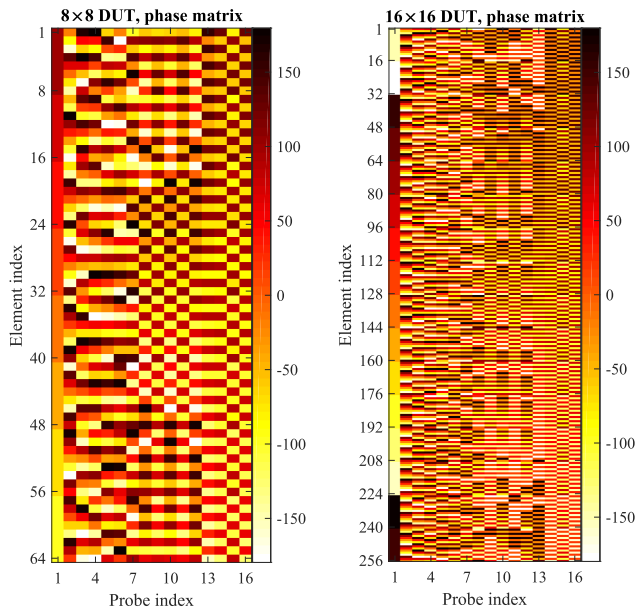**FIGURE 3.** Target PAS of CDL-C channel model and virtual probe locations (white dots).

FIGURE 4. Phase information (with unit of degree) in the phase matrix for 16 virtual probes and two DUTs.

FIGURE 5. Power weights of 16 virtual probes for 8 × 8 DUT as an example.
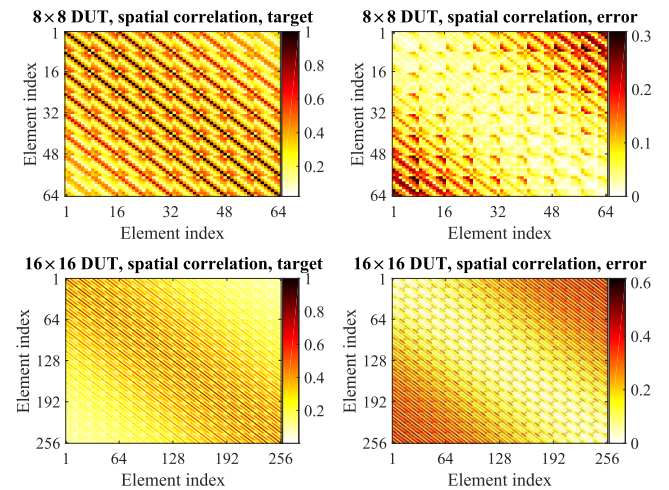
FIGURE 6. Target spatial correlation and the correlation error for two DUTs.

The corresponding phase information of the phase matrix for two DUTs is given in Fig. 4 with the unit of degrees. Different probe locations produce different array responses at the DUTs. As presented in Section III-A, the first probe location is allocated at the AoD and EoD of the strongest cluster in the target channel model. For the CDL-C channel model, the azimuth angle of the first probe is nearly 0°. As a result, the phase rotation is identical on every 8 and 16 elements with the same elevation angle for a 8 × 8 DUT and a 16 × 16 DUT, respectively. Fig. 5 displays an example of power weights of 16 virtual probes for a 8 × 8 DUT. The normalized power weights for each cluster are presented, which can be accurately generated in the CE.

B. EMULATION ACCURACY

The results of the target spatial correlation $|\rho_q|$ and the spatial correlation error $|\rho_q - \hat{\rho}_q|$ for two DUTs are shown in Fig. 6. It can be found that the emulated spatial correlation $|\hat{\rho}_q|$ matches well with the target spatial correlation $|\rho_q|$ in the region where the element distance is small. While the error
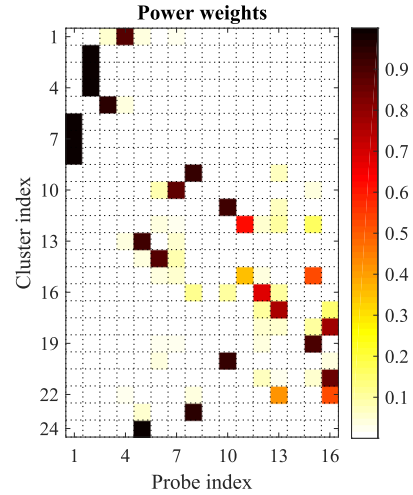
$|\rho_q - \hat{\rho}_q|$ increases in the region where the element distance is large. Statistics of weighted rms correlation error e_ρ for two DUTs are summarized in Table 2.

Fig. 7 displays the estimated PAS by two DUTs using Bartlett beamforming under the target channel $P_{est}(\Omega)$ and the emulated channel $\hat{P}_{est}(\Omega)$. With the limited DUT size (e.g. 8 × 8), the estimated PAS is similar under the target and the emulated channel. While the similarity of estimated PAS decreases with the increase of DUT size (e.g. 16 × 16). In Table 2 is summarized the statistics of PAS estimate error D_{est} between the target and the emulated channel for two DUTs.

The beam probability distribution under the target channel p_b and the emulated channel $\hat{p}_b$ for two DUTs is demonstrated in Fig. 8. Like the PAS estimate, the beam probability distribution is similar under the target and the emulated channel with limited DUT size. While the similarity of beam probability distribution reduces with the increased DUT size.
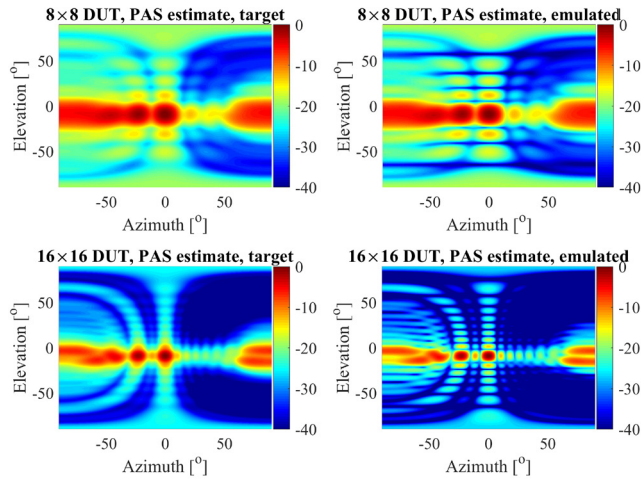
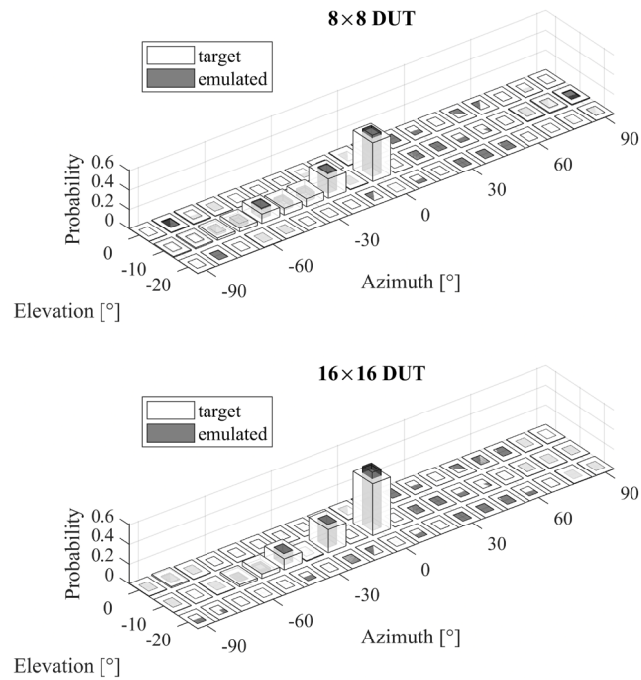**FIGURE 7.** PAS estimate under the target and the emulated channel for two DUTs.

FIGURE 8. Beam probability distributions under the target and the emulated channel for two DUTs.

TABLE 2. Statistics of three evaluation metrics for two DUTs.

DUT size	e_ρ	D_{est}	D_{beam}
8×8	0.093	0.062	0.053
16×16	0.189	0.161	0.075

In Table 2 is summarized the statistics of beam statistical distance D_{beam} for two DUTs.

It can be found from Table 2 that good emulation accuracy is obtained for a certain DUT size, while it degrades with increasing DUT size in terms of the spatial correlation,

the PAS estimate, and the beam probability. As evaluation metrics, their performance is degraded for larger DUT size under limited setup configurations, as expected, i.e. larger DUT has stronger capability to distinguish the target and the emulated channel.

V. CONCLUSION

In this paper, we have discussed the challenges of 3D sectored MPAC setups in existence for massive MIMO BS testing and proposed a concept of virtual OTA testing based on MPAC setups. The virtual OTA testing is reflected in the virtual probes, which substitute the actual probes of MPAC setups in a phase matrix of the proposed virtual OTA test system. Knowing from the two categories of methods for the performance testing of a 5G massive MIMO BS (i.e. conductive test and OTA test), the proposed virtual OTA testing has potential values in the future. On the one hand, the required fading channels are much fewer than they are in the conventional conductive testing. Compared with the MPAC OTA testing, on the other hand, it reduces the complexity and inconvenience of sectored MPAC setup in terms of OTA probes for massive MIMO BS testing, with arbitrary virtual probe locations achieved flexibly. Simultaneously, the required number of fading channels does not increase. As a future work one could investigate the practical aspects of the virtual OTA test system, e.g. the practical implementation of the programmable phase matrix, and the connection between the DUT array and the phase matrix.

APPENDIX A
DERIVATION OF TARGET SPATIAL CORRELATION
A. SINGLE-CLUSTER CHANNEL MODEL

For the single cluster l, the target spatial correlation $\rho_q^{(l)}$ at any pair $q = (u, v)$ of spatial locations $\overrightarrow{r_u}$ and $\overrightarrow{r_v}$ for DUT element u and v respectively ($u, v \in [1, M]$) is calculated by

$$
\begin{aligned}
\rho_q^{(l)} &= \frac{1}{\mu_l} E\left\{ x_u^{(l)}(t) \cdot x_v^{(l)}(t)^* \right\} \\
&= \frac{1}{\mu_l} E\Bigg\{ \oint e^{j\frac{2\pi}{\lambda}\overrightarrow{r_u}\cdot\overrightarrow{\Omega}} \sqrt{P^{(l)}(\Omega)} e^{j\varphi_\Omega(t)} \, d\Omega \\
&\quad \cdot \oint e^{-j\frac{2\pi}{\lambda}\overrightarrow{r_v}\cdot\overrightarrow{\Omega'}} \sqrt{P^{(l)}(\Omega')} e^{-j\varphi_{\Omega'}(t)} \, d\Omega' \Bigg\} \\
&= \frac{1}{\mu_l} E\Bigg\{ \oint\oint e^{j\frac{2\pi}{\lambda}(\overrightarrow{r_u}\cdot\overrightarrow{\Omega} - \overrightarrow{r_v}\cdot\overrightarrow{\Omega'})} \sqrt{P^{(l)}(\Omega)P^{(l)}(\Omega')} \\
&\quad \cdot e^{j(\varphi_\Omega(t) - \varphi_{\Omega'}(t))} \, d\Omega \, d\Omega' \Bigg\} \\
&= \frac{1}{\mu_l} E\Big\{ x_u^{(l)}(t) \cdot x_v^{(l)}(t)^*\big|_{\Omega=\Omega'} \\
&\quad + x_u^{(l)}(t) \cdot x_v^{(l)}(t)^*\big|_{\Omega\neq\Omega'} \Big\}.
\end{aligned}
\tag{17}
$$

Since we have

$$
E\left\{ e^{j(\varphi_\Omega(t) - \varphi_{\Omega'}(t))} \right\} = \begin{cases} 1 & \text{when } \Omega = \Omega' \\ 0 & \text{when } \Omega \neq \Omega' \end{cases},
\tag{18}
$$

(17) can be simplified to

$$\rho_q^{(l)} = \frac{1}{\mu_l} E\left\{ x_u^{(l)}(t) \cdot x_v^{(l)}(t)^* \big|_{\Omega=\Omega'} \right\}$$

$$= \frac{1}{\mu_l} \oint e^{j\frac{2\pi}{\lambda}(\vec{r_u} - \vec{r_v}) \cdot \vec{\Omega}} P^{(l)}(\Omega) \, d\Omega. \quad (19)$$

To satisfy $\rho_q^{(l)} = 1$ when $u = v$, we have

$$\mu_l = \oint P^{(l)}(\Omega) \, d\Omega = P_l. \quad (20)$$

Then

$$\rho_q^{(l)} = \frac{1}{P_l} \oint e^{j\frac{2\pi}{\lambda}(\vec{r_u} - \vec{r_v}) \cdot \vec{\Omega}} P^{(l)}(\Omega) \, d\Omega. \quad (21)$$

B. MULTI-CLUSTER CHANNEL MODEL
For multiple clusters, we have

$$\rho_q = \frac{1}{\mu} E\left\{ x_u(t) \cdot x_v(t)^* \right\}$$

$$= \frac{1}{\mu} E\left\{ \sum_{l=1}^{L} x_u^{(l)}(t) \cdot \left(\sum_{l'=1}^{L} x_v^{(l')}(t) \right)^* \right\}$$

$$= \frac{1}{\mu} E\left\{ \sum_{l'=1}^{L} \sum_{l=1}^{L} x_u^{(l)}(t) \cdot x_v^{(l')}(t)^* \right\}$$

$$= \frac{1}{\mu} \sum_{l'=1}^{L} \sum_{l=1}^{L} E\left\{ x_u^{(l)}(t) \cdot x_v^{(l')}(t)^* \right\}. \quad (22)$$

According to (17)~(19) in Appendix A-A, we can obtain

$$E\left\{ x_u^{(l)}(t) \cdot x_v^{(l')}(t)^* \right\}$$

$$= \oint e^{j\frac{2\pi}{\lambda}(\vec{r_u} - \vec{r_v}) \cdot \vec{\Omega}} \sqrt{P^{(l)}(\Omega) P^{(l')}(\Omega)} \, d\Omega. \quad (23)$$

Then

$$\rho_q = \frac{1}{\mu} \sum_{l'=1}^{L} \sum_{l=1}^{L} \oint e^{j\frac{2\pi}{\lambda}(\vec{r_u} - \vec{r_v}) \cdot \vec{\Omega}} \sqrt{P^{(l)}(\Omega) P^{(l')}(\Omega)} \, d\Omega. \quad (24)$$

To satisfy $\rho_q = 1$ when $u = v$, we have

$$\mu = \sum_{l'=1}^{L} \sum_{l=1}^{L} \oint \sqrt{P^{(l)}(\Omega) P^{(l')}(\Omega)} \, d\Omega. \quad (25)$$

APPENDIX B
DERIVATION OF EMULATED SPATIAL CORRELATION
A. SINGLE-CLUSTER CHANNEL MODEL
For the single cluster l, the emulated spatial correlation $\hat{\rho}_q^{(l)}$ at locations pair q is calculated by

$$\hat{\rho}_q^{(l)} = \frac{1}{\hat{\mu}_l} E\left\{ \hat{x}_u^{(l)}(t) \cdot \hat{x}_v^{(l)}(t)^* \right\}$$

$$= \frac{1}{\hat{\mu}_l} E\left\{ \sum_{k=1}^{K} e^{j\frac{2\pi}{\lambda} \vec{r_u} \cdot \vec{\hat{\Omega}}_k} \sqrt{\hat{P}_k^{(l)}} e^{j\varphi_k(t)} \right.$$

$$\cdot \sum_{k'=1}^{K} e^{-j\frac{2\pi}{\lambda} \vec{r_v} \cdot \vec{\hat{\Omega}}_{k'}} \sqrt{\hat{P}_{k'}^{(l)}} e^{-j\varphi_{k'}(t)} \Bigg\}$$

$$= \frac{1}{\hat{\mu}_l} \left\{ \sum_{k'=1}^{K} \sum_{k=1}^{K} e^{j\frac{2\pi}{\lambda}(\vec{r_u} \cdot \vec{\hat{\Omega}}_k - \vec{r_v} \cdot \vec{\hat{\Omega}}_{k'})} \sqrt{\hat{P}_k^{(l)} \hat{P}_{k'}^{(l)}} \right.$$

$$\cdot e^{j(\varphi_k(t) - \varphi_{k'}(t))} \Bigg\}$$

$$= \frac{1}{\hat{\mu}_l} E\left\{ \hat{x}_u^{(l)}(t) \cdot \hat{x}_v^{(l)}(t)^* \big|_{k=k'} \right.$$

$$+ \hat{x}_u^{(l)}(t) \cdot \hat{x}_v^{(l)}(t)^* \big|_{k \neq k'} \Bigg\}. \quad (26)$$

Since we have

$$E\left\{ e^{j(\varphi_k(t) - \varphi_{k'}(t))} \right\} = \begin{cases} 1 & \text{when } k = k' \\ 0 & \text{when } k \neq k', \end{cases} \quad (27)$$

(26) can be simplified to

$$\hat{\rho}_q^{(l)} = \frac{1}{\hat{\mu}_l} E\left\{ \hat{x}_u^{(l)}(t) \cdot \hat{x}_v^{(l)}(t)^* \big|_{k=k'} \right\}$$

$$= \frac{1}{\hat{\mu}_l} \sum_{k=1}^{K} \hat{P}_k^{(l)} \cdot e^{j\frac{2\pi}{\lambda}(\vec{r_u} - \vec{r_v}) \cdot \vec{\hat{\Omega}}_k}. \quad (28)$$

To satisfy $\hat{\rho}_q^{(l)} = 1$ when $u = v$, we have

$$\hat{\mu}_l = \sum_{k=1}^{K} \hat{P}_k^{(l)} = P_l. \quad (29)$$

Then

$$\hat{\rho}_q^{(l)} = \sum_{k=1}^{K} w_k^{(l)} \cdot e^{j\frac{2\pi}{\lambda}(\vec{r_u} - \vec{r_v}) \cdot \vec{\hat{\Omega}}_k}, \quad (30)$$

where $w_k^{(l)} = \hat{P}_k^{(l)}/P_l$.

B. MULTI-CLUSTER CHANNEL MODEL
For multiple clusters, we have

$$\hat{\rho}_q = \frac{1}{\hat{\mu}} E\left\{ \hat{x}_u(t) \cdot \hat{x}_v(t)^* \right\}$$

$$= \frac{1}{\mu} E\left\{ \sum_{l=1}^{L} \hat{x}_u^{(l)}(t) \cdot \left(\sum_{l'=1}^{L} \hat{x}_v^{(l')}(t) \right)^* \right\}$$

$$= \frac{1}{\mu} E\left\{ \sum_{l'=1}^{L} \sum_{l=1}^{L} \hat{x}_u^{(l)}(t) \cdot \hat{x}_v^{(l')}(t)^* \right\}$$

$$= \frac{1}{\mu} \sum_{l'=1}^{L} \sum_{l=1}^{L} E\left\{ \hat{x}_u^{(l)}(t) \cdot \hat{x}_v^{(l')}(t)^* \right\}. \quad (31)$$

According to (26)~(28) in Appendix B-A, we can obtain

$$E\left\{ \hat{x}_u^{(l)}(t) \cdot \hat{x}_v^{(l')}(t)^* \right\} = \sum_{k=1}^{K} \sqrt{\hat{P}_k^{(l)} \hat{P}_k^{(l')}} \cdot e^{j\frac{2\pi}{\lambda}(\vec{r_u} - \vec{r_v}) \cdot \vec{\hat{\Omega}}_k}. \quad (32)$$

Since $\hat{P}_k^{(l)} = w_k^{(l)} P_l$ and $\hat{P}_k^{(l')} = w_k^{(l')} P_{l'}$, we have

$$\hat{\rho}_q = \frac{1}{\hat{\mu}} \sum_{l'=1}^{L} \sum_{l=1}^{L} \sum_{k=1}^{K} \sqrt{P_l P_{l'}} \sqrt{w_k^{(l)} w_k^{(l')}} \cdot e^{j\frac{2\pi}{\lambda}(\vec{r_u} - \vec{r_v}) \cdot \vec{\hat{\Omega}}_k}. \quad (33)$$

To satisfy $\hat{\rho}_q = 1$ when $u = v$, we have

$$\hat{\mu} = \sum_{l'=1}^{L} \sum_{l=1}^{L} \sum_{k=1}^{K} \sqrt{P_l P_{l'}} \sqrt{w_k^{(l)} w_k^{(l')}}. \qquad (34)$$

REFERENCES

[1] *Study on New Radio Access Technology: Physical Layer Aspects*, document TR 38.802, Version 14.2.0, 3GPP, Sep. 2017.

[2] *Study on New Radio Access Technology: Radio Interface Protocol Aspects*, document TR 38.804, Version 14.0.0, 3GPP, Mar. 2017.

[3] A. Osseiran, J. F. Monserrat, and P. Marsch, *5G Mobile and Wireless Communications Technology*. Cambridge, U.K.: Cambridge Univ. Press, Jun. 2016.

[4] E. G. Larsson, O. Edfors, F. Tufvesson, and T. L. Marzetta, "Massive MIMO for next generation wireless systems," *IEEE Commun. Mag.*, vol. 52, no. 2, pp. 186–195, Feb. 2014.

[5] X. Gao, O. Edfors, F. Rusek, and F. Tufvesson, "Massive MIMO performance evaluation based on measured propagation data," *IEEE Trans. Wireless Commun.*, vol. 14, no. 7, pp. 3899–3911, Jul. 2015.

[6] A. O. Martínez, J. Ø. Nielsen, E. De Carvalho, and P. Popovski, "An experimental study of massive MIMO properties in 5G scenarios," *IEEE Trans. Antennas Propag.*, vol. 66, no. 12, pp. 7206–7215, Dec. 2018.

[7] M. Rumney, R. Pirkl, M. H. Landmann, and D. A. Sanchez-Hernandez, "MIMO over-the-air research, development, and testing," *Int. J. Antennas Propag.*, vol. 2012, May 2012, Art. no. 467695.

[8] P. Kyösti, T. Jämsä, and J.-P. Nuutinen, "Channel modelling for multi-probe over-the-air MIMO testing," *Int. J. Antennas Propag.*, vol. 2012, Mar. 2012, Art. no. 615954.

[9] M. D. Foegelle, "The future of MIMO over-the-air testing," *IEEE Commun. Mag.*, vol. 52, no. 9, pp. 134–142, Sep. 2014.

[10] D. Reed, A. Rodriguez-Herrera, and R. Borsato, "Measuring massive MIMO array systems using over the air techniques," in *Proc. 11th Eur. Conf. Antennas Propag. (EUCAP)*, Mar. 2017, pp. 3663–3667.

[11] M. Gustafsson, T. Jämsä, and M. Högberg, "OTA methods for 5G BTS testing—Survey of potential approaches," in *Proc. 32nd Gen. Assem. Sci. Symp. Int. Union Radio Sci. (URSI GASS)*, Aug. 2017, pp. 1–4.

[12] P. Zhang, X. Yang, J. Chen, and Y. Huang, "A survey of testing for 5G: Solutions, opportunities, and challenges," *China Commun.*, vol. 16, no. 1, pp. 69–85, Jan. 2019.

[13] P.-S. Kildal and K. Rosengren, "Correlation and capacity of MIMO systems and mutual coupling, radiation efficiency, and diversity gain of their antennas: Simulations and measurements in a reverberation chamber," *IEEE Commun. Mag.*, vol. 42, no. 12, pp. 104–112, Dec. 2004.

[14] X. Chen, "Throughput modeling and measurement in an isotropic-scattering reverberation chamber," *IEEE Trans. Antennas Propag.*, vol. 62, no. 4, pp. 2130–2139, Apr. 2014.

[15] W. Yu, Y. Qi, K. Liu, Y. Xu, and J. Fan, "Radiated two-stage method for LTE MIMO user equipment performance evaluation," *IEEE Trans. Electromagn. Compat.*, vol. 56, no. 6, pp. 1691–1696, Dec. 2014.

[16] W. Fan, P. Kyösti, L. Hentilä, and G. F. Pedersen, "MIMO terminal performance evaluation with a novel wireless cable method," *IEEE Trans. Antennas Propag.*, vol. 65, no. 9, pp. 4803–4814, Sep. 2017.

[17] H. Gao, W. Wang, W. Fan, Y. Wu, Y. Liu, and G. F. Pedersen, "Over-the-air testing for carrier aggregation enabled MIMO terminals using radiated two-stage method," *IEEE Access*, vol. 6, pp. 71622–71631, Nov. 2018.

[18] W. Fan, I. Carton, P. Kyösti, A. Karstensen, T. Jämsä, M. Gustafsson, and G. F. Pedersen, "A step toward 5G in 2020: Low-cost OTA performance evaluation of massive MIMO base stations," *IEEE Antennas Propag. Mag.*, vol. 59, no. 1, pp. 38–47, Feb. 2017.

[19] P. Kyösti, W. Fan, G. F. Pedersen, and M. Latva-Aho, "On dimensions of OTA setups for massive MIMO base stations radiated testing," *IEEE Access*, vol. 4, pp. 5971–5981, Sep. 2016.

[20] P. Kyösti, W. Fan, and J. Kyröläinen, "Assessing measurement distances for OTA testing of massive MIMO base station at 28 GHz," in *Proc. 11th Eur. Conf. Antennas Propag. (EUCAP)*, Mar. 2017, pp. 3679–3683.

[21] F. Zhang, W. Fan, Y. Ji, M. Gustafsson, T. Jamsa, G. Steinböck, P. Kyösti, and G. F. Pedersen, "Performance testing of massive MIMO base station with multi-probe anechoic chamber setups," in *Proc. 12th Eur. Conf. Antennas Propag. (EuCAP)*, Apr. 2018, pp. 1–5.

[22] P. Kyösti, L. Hentilä, W. Fan, J. Lehtomäki, and M. Latva-Aho, "On radiated performance evaluation of massive MIMO devices in multiprobe anechoic chamber OTA setups," *IEEE Trans. Antennas Propag.*, vol. 66, no. 10, pp. 5485–5497, Oct. 2018.

[23] *Study on Channel Model for Frequencies From 0.5 to 100 GHz*, document TR 38.901, Version 15.0.0, 3GPP, Jul. 2018.

[24] D. Reed, A. Rodríguez-Herrera, and J.-P. Nuutinen, "Massive MIMO array testing using a programmable phase matrix and channel emulator," in *Proc. 12th Eur. Conf. Antennas Propag. EuCAP)*, Apr. 2018, pp. 1–4.

[25] W. Fan, F. Sun, J. Ø. Nielsen, X. Carreño, J. S. Ashta, M. B. Knudsen, and G. F. Pedersen, "Probe selection in multiprobe OTA setups," *IEEE Trans. Antennas Propag.*, vol. 62, no. 4, pp. 2109–2120, Apr. 2014.

[26] Y. Ji, W. Fan, G. F. Pedersen, and X. Wu, "On channel emulation methods in multi-probe anechoic chamber setups for over-the-air testing," *IEEE Trans. Veh. Technol.*, vol. 67, no. 8, pp. 6740–6751, Aug. 2018.

[27] P. Kyösti, L. Hentilä, J. Kyröläinen, F. Zhang, W. Fan, and M. Latva-Aho, "Emulating dynamic radio channels for radiated testing of massive MIMO devices," in *Proc. 12th Eur. Conf. Antennas Propag. (EuCAP)*, Apr. 2018, pp. 1–5.

[28] S. Boyd and L. Vandenberghe, *Convex Optimization*. Cambridge, U.K.: Cambridge Univ. Press, Mar. 2004.

[29] W. Fan, P. Kyösti, J. Ø. Nielsen, and G. F. Pedersen, "Wideband MIMO channel capacity analysis in multiprobe anechoic chamber setups," *IEEE Trans. Veh. Technol.*, vol. 65, no. 5, pp. 2861–2871, May 2016.

[30] P. Stoica and R. L. Moses, *Spectral Analysis of Signals*. Upper Saddle River, NJ, USA: Prentice-Hall, Jul. 2005.

[31] W. Fan, P. Kyösti, M. Rumney, X. Chen, and G. F. Pedersen, "Over-the-air radiated testing of millimeter-wave beam-steerable devices in a cost-effective measurement setup," *IEEE Commun. Mag.*, vol. 56, no. 7, pp. 64–71, Jul. 2018.

[32] H. Gao, W. Wang, W. Fan, Y. Wu, Y. Liu, and G. F. Pedersen, "Beam probability metric for OTA testing of adaptive antenna systems in multi-probe anechoic chamber setups," in *Proc. 13th Eur. Conf. Antennas Propag. (EuCAP)*, Apr. 2019, pp. 1–5.
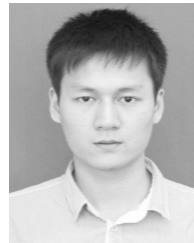
HUAQIANG GAO received the B.E. degree in electronic and information engineering from the Harbin University of Science and Technology and the B.A. degree in business English from Heilongjiang University, Harbin, China, in 2016. He is currently pursuing the Ph.D. degree in electronic science and technology with the Beijing University of Posts and Telecommunications, Beijing, China. Since 2018, he has been a Research Intern with the Antennas, Propagation and Millimeter-wave Systems Section, Aalborg University. His research interest includes over the air testing of wireless devices.

WEIMIN WANG received the B.S. degree in communication engineering, the M.S. degree, and the Ph.D. degree in electronic engineering from the Beijing University of Posts and Telecommunications (BUPT), Beijing, China, in 1999, 2004, and 2014, respectively. In 2014, she joined the BUPT, where she is currently an Associate Professor with the School of Electronic Engineering. Her research interests include electromagnetic field and MIMO OTA measurement.

YONGLE WU received the B.Eng. degree in communication engineering and the Ph.D. degree in electronic engineering from the Beijing University of Posts and Telecommunications (BUPT), Beijing, China, in 2006 and 2011, respectively. From April to October 2010, he was a Research Assistant with the City University of Hong Kong (CityU), Hong Kong. In 2011, he joined the BUPT, where he is currently a Full Professor with the School of Electronic Engineering. His research interests include microwave components and wireless systems design.

YUANAN LIU received the B.E., M.Eng., and Ph.D. degrees in electrical engineering from the University of Electronic Science and Technology of China, Chengdu, China, in 1984, 1989, and 1992, respectively. In 1984, he joined the 26th Institute of Electronic Ministry of China to develop the inertia navigating system. In 1992, he began his first Postdoctoral position at the EMC Lab., Beijing University of Posts and Telecommunications (BUPT), Beijing, China. In 1995, he started his second Postdoctoral with the Broadband Mobile Lab, Department of System and Computer Engineering, Carleton University, Ottawa, Canada. Since July 1997, he has been a Professor with the Wireless Communication Center, College of Telecommunication Engineering, BUPT, Beijing, where he is involved in the development of next-generation cellular systems, wireless LANs, Bluetooth application for data transmission, EMC design strategies for high speed digital systems, and EMI and EMS measuring sites with low cost and high performance.

GERT FRØLUND PEDERSEN was born in 1965. He received the B.Sc. degree (Hons.) in electrical engineering from the College of Technology, Dublin, Ireland, in 1991, and the M.Sc. degree in electrical engineering and the Ph.D. degree from Aalborg University, in 1993 and 2003, respectively. He has been with Aalborg University, since 1993, where he is currently a Full Professor heading the Antenna, Propagation and Networking Laboratory with 36 researchers. He is also the Head of the doctoral school on wireless communication with some 100 Ph.D. students enrolled. He has also involved as a consultant for developments of more than 100 antennas for mobile terminals, including the first internal antenna for mobile phones with lowest SAR, in 1994, first internal triple-band antenna, in 1998, with low SAR and high TRP and TIS, and lately various multi-antenna systems rated as the most efficient on the market. He has involved with joint university and industry projects most of the time and has received more than 12 M\$ in direct research funding. Latest, he is the Project Leader of the SAFE Project with a total budget of 8 M\$ investigating tunable front end, including tunable antennas for the future multiband mobile phones. He has been one of the pioneers in establishing over-the-air (OTA) measurement systems. The measurement technique is now well established for mobile terminals with single antennas and he was chairing the various COST groups (swg2.2 of COST 259, 273, 2100, and now ICT1004) with liaison to 3GPP for OTA test of MIMO terminals. He is also deeply involved in MIMO OTA measurement. He has published over 175 peer-reviewed papers and holds 28 patents. His research has focused on radio communication for mobile terminals, especially small antennas, diversity systems, and propagation and biological effects.

● ● ●